Transactions of the Korean Nuclear Society Spring Meeting
Jeju, Korea, May 18-19, 2017

External loss analysis of a supercritical CO_2 radial compressor

Seong Gu Kim[a], Seong Kuk Cho[a], Jeong Ik Lee[a], Jekyoung Lee[b], Si Woo Lee[b], Yacine Addad[c], Jae Eun Cha[d]
[a]*Dept. Nuclear & Quantum Eng., KAIST, 373-1, Guseong-dong, Yuseong-gu, Daejeon, 305-701, Republic of Korea*
Jinsol Turbo, Gwanpyeong-dong 695, Yuseong-gu, Daejeon, Republic of Korea
Khalifa University of Science, Technology & Research (KUSTAR), P.O.Box 127788, Abu Dhabi, UAE
Korea Atomic Energy Research Institute (KAERI), 150-1, Dukjin-dong, Yuseong-gu, Daejeon, Republic of Korea
**Corresponding author : jeongiklee@kaist.ac.kr*

1. Introduction

The supercritical CO_2 Brayton cycle (S-CO_2 cycle) technology is being actively developed in many research institutes because it has many advantages and potential to replace existing steam Rankine cycles. The S-CO_2 cycle can be used for various heat sources such as Gen IV nuclear reactors, concentrated solar power (CSP), and coal power plants. It has a small footprint due to the compact turbomachine and heat exchangers [1]. It was found that the S-CO_2 compressor consumes small compression work if the operating conditions approach to the critical point. Therefore, this reduced compression work contributes to high cycle efficiency.

To demonstrate the S-CO_2 cycle performance, an integral test facility was constructed. The joint research team of KAERI, KAIST and POSTECH designed a supercritical CO_2 integral experiment loop (SCIEL) [2].

The experimental data from the SCIEL loop are being accumulated for various conditions and rotational speeds. Design condition of the compressor is 70,000rpm and 1.8 pressure ratio. The design & manufacturing of this compressor was conducted by Jinsol Turbo Inc.

In this study, 3-D Reynolds-Averaged Navier Stokes (RANS) simulation was performed to investigate the SCIEL compressor. The fluid domain of rotor and stator was made. The real gas properties of S-CO_2 were implemented as a CSV format table. With the 3-D CFD approach, the authors intended to observe internal flow which provides crucial information for compressor design. In addition, the loss mechanism of a compressor can be understood better with the CFD analysis. The results obtained from SCIEL loop were compared to the CFD result. After an extraction of external losses from the experimental results, a set of external loss models was proposed.

2. SCIEL LOOP

The main on-design variables of compressor are shown in Table 1. SCIEL compressor has a shrouded impeller. On the design point, each impeller consumes 50kW power. Fig. 1 shows the twin impeller configuration, and leakage flows passing through backward disk of impeller. This leakage flows result in external losses at the bearings, rotor. The thrust bearing uses end surface of rotor as a rotating support part without thrust collar. Leakage flows of twin impellers are merged in the middle section of the stator and drains into the loop.

Table 1. Design variables of compressor [3].

Design variables	
Total inlet temperature	33℃
Total inlet pressure	7.8MPa
Pressure ratio	1.8
Mass flow rate	3.2kg/s (each side)
Total to total efficiency	65%
Number of vanes	16
Shaft speed	70,000rpm

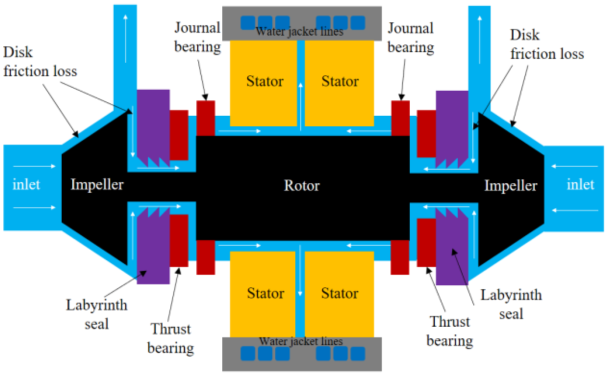

Fig. 1. Flow paths of the compressor.

3. Analysis Model

A commercial CFD code, Star-CCM+ V10.06 was used for the CFD analysis [3]. For the turbulence modeling, the k-ω SST model with wall function was used [4]. This model is considered as a most promising option for turbomachine analysis. It is known that this model returns accurate results among the two-equation turbulence models [5]. The internal compressor geometry including ring diffuser, outlet diffuser and volute casing was used to generate fluid domain. However, external flow paths such as disk gap, leakage, and rotor cavity were not included due to the computational limit and numerical instability. The fluid domain was divided into rotor and stator parts. The interfacial surfaces are connected by mixing-plane approach [6]. In this method, circumferential averaged flow variables on both sides are coupled at the interface.

For the property implementation of supercritical CO_2, the CSV table was made with a simple MATLAB code. This table contains properties at the given pressure, temperature columns. The table contains density, dynamic viscosity, enthalpy, entropy, speed of sound, and thermal conductivity. All the property errors are less than 0.1% except for specific heat in constant pressure (2%). The table mainly used for simulation has ranges of 0.1-20MPa, 253-2000K with 5,000 by 5,000 resolution. The tables have wide pressure, temperature ranges in order to improve numerical stability in iterations.

The Grid Convergence Index (GCI) was used for examining the grid independence as summarized in Table 1. The GCI method is the most reliable method for the prediction of grid uncertainty [7]. This method is based on Richardson extrapolation. The output variables such as torque acting on the impeller and total-to-total pressure ratio are considered as critical variables. After that, a fine mesh system with 1,391,350 cells was chosen for CFD analysis. The numerical uncertainty in the fine grid solutions for compressor performance is 0.07%.

If we estimate an isentropic efficiency based on the enthalpy form (ideal enthalpy rise) / (real enthalpy rise), the unstable value of denominator leads to nonphysical isentropic efficiency. Therefore, to obtain isentropic efficiency in more stable way, an energy balance form was used.

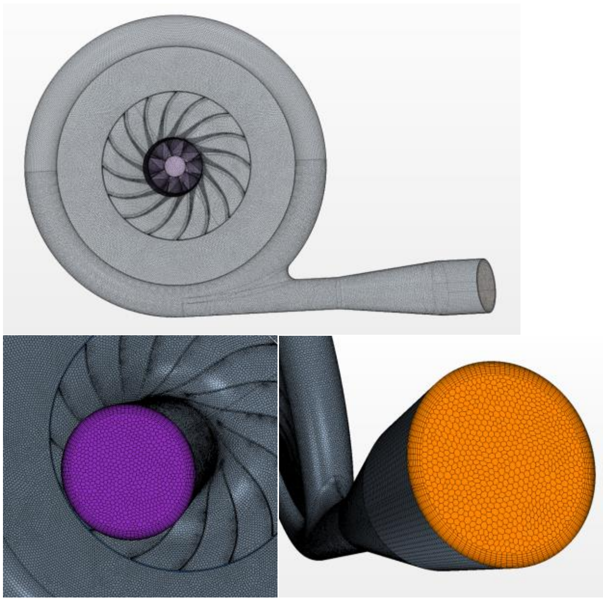

Fig. 2. Mesh shape of compressor.

Table 2. Grid Convergence Index (GCI).

	ϕ = Torque	ϕ = Total to total pressure ratio
N_1, N_2, N_3	1,391,350, 725,983, 486,159	
r_{21}	1.2409	1.2409
r_{32}	1.1415	1.1415
Φ_1	1.160455	1.1053
Φ_2	1.163899	1.1072
Φ_3	1.141289	1.1100
P	13.421	5.2057
ϕ_ext	1.16025	1.1049
GCI_{fine}	0.052%	0.0727%

4. Problem Setup

The inlet conditions of 7.8-8.0MPa, 40-42℃ and various outlet conditions from the experiment were utilized as boundary conditions. At the inlet boundary, 1% of turbulence intensity was prescribed. The rotational speeds in the experiment are in the range of 25,000-35,000rpm. For the given inlet and outlet conditions, mass flow rate and torque acting on the impeller surface were obtained after calculation as the output variables.

The residual of mass, momentum, and energy, and turbulent kinetic energy, turbulent dissipation frequency were monitored. Furthermore, mass flowrate and temperature at the outlet were checked to ensure the solution to obtain an accurate solution.

5. Result

Numerical results and experimental data of total-to-total pressure ratio and isentropic efficiency were compared. The obtained mass flow rate was converted to flow coefficient form.

The internal losses are related to the pressure ratio performance of a compressor. The mechanical energy of rotating impeller is transferred to the enthalpy of fluid [8]. However, internal losses consume some portion of enthalpy during this process. Therefore, the internal losses are the major factor for the pressure ratio curves. On the other hand, external losses are related to the compressor efficiency because the losses are defined as the loss occurred at the exterior flow path of the compressor. The external losses increase the input work to rotate the impeller.

The authors found that there is a large discrepancy between a stage efficiency obtained in CFD analysis and experimental result because the fluid domain used in analysis excludes external flow paths. Therefore, the amount of external losses was estimated by using energy balance of the machine. In addition, appropriate external loss models were utilized to compare the results.

At first, the measured external loss was obtained from equation (1). Experimental uncertainty on the external loss was found and shown in the Figures 3-5 with uncertainty bands. Also, the external loss models were used to estimate external losses in given geometry, and flow parameters.

The estimated external loss located inside the uncertainty band of measured loss. The authors found that the windage loss occupies 89-93% of the external loss. Disk friction and bearing loss are quite low since the disk area and end surface of rotor is small. As for the uncertainty band range, it has wide range since the temperature of leakage outlet line is unknown. Also, amount of heat based on enthalpy difference measured with temperature and pressure results in high uncertainty close to critical point. As a result, this set of external loss models for S-CO_2 compressor predicts accurate power loss.

$$W_{loss.ext} = W_{input} - H_{co2} - Q_{water} - Q_{leak} \quad - - - (1)$$

Where, $W_{loss} = W_{disk}+W_{windage}+W_{bearing}$ - - - (2)

The external loss models are shown as follows:

i) Disk friction (Daily and Nece) [9]:

$$\Delta h_{disk} = C_m \frac{\rho_{avg} r_2^2 U_2^3}{4\dot{m}} \quad \text{- - - - - (3)}$$

$$C_m = \frac{0.102(s/a)^{0.1}}{\mathrm{Re}_{disk}^{0.2}} \quad \text{- - - - - (4)}$$

(Regime IV, Turbulent flow, separate boundary layers),

$$\mathrm{Re}_{disk} = \frac{\rho_2 U_2 r_2}{\mu_2}$$

ii) Front side disk friction with slope (Gülich) [10]:

$$\Delta h_{disk} = \frac{C_m}{4\dot{m}\cos\delta} \rho \omega^3 r_2^5 \left[1 - \left(\frac{r_i}{r_2}\right)^5\right] \quad \text{- - - - - (5)}$$

iii) Windage loss (Vrancik) [11]:

$$W_{windage} = \pi C_d \rho_{cavity} r_{rotor}^4 \omega^3 L \quad \text{- - - - - (6)}$$

$$\frac{1}{\sqrt{C_d}} = 2.04 + 1.768 \ln(\mathrm{Re}\sqrt{C_d})$$

Where $\mathrm{Re}_{rotor} = \dfrac{\rho_{rotor} r_{rotor} t_{gap} \omega}{\mu}$

iv) Bearing loss (Schlichting) [12]:

$$P_{turb} = 0.0156 \rho^{0.8} \omega^{2.8} r_o^{-0.4} (r_o^5 - r_i^5) / \mu^{-0.2} \quad \text{- - - - - (7)}$$

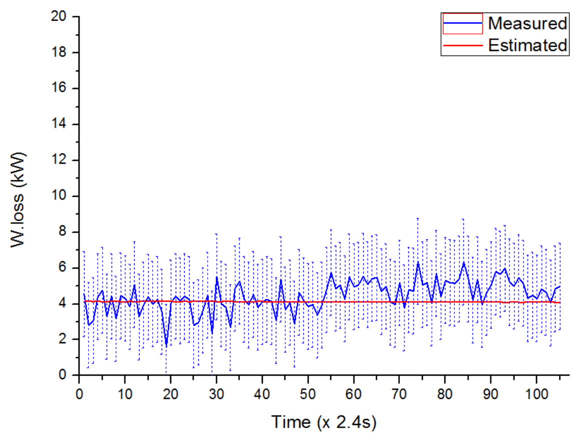

Fig. 3. Measured external loss compared to estimated loss at 25,000rpm.

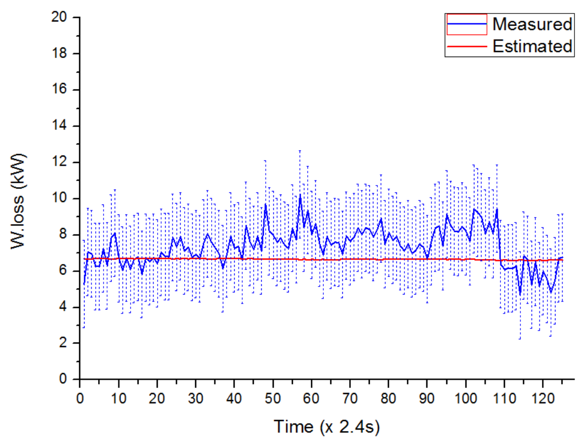

Fig. 4. Measured external loss compared to estimated loss at 30,000rpm.

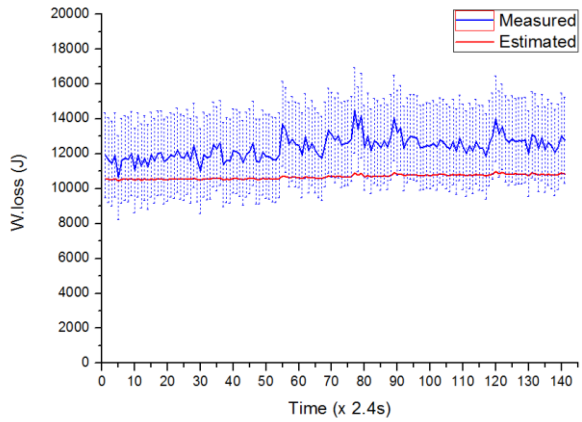

Fig. 5. Measured external loss compared to estimated loss at 35,000rpm.

The CFD result of pressure ratio versus flow coefficient showed similar characteristic when compared to the experimental curve as shown in Fig. 6. It means that the analysis model successfully captures the internal geometrical, physical characteristic of the flow. Fig. 7 shows total-to-total isentropic efficiency curves versus flow coefficient. The stage efficiency without external flow path showed large discrepancy when compared to the experimental efficiency. Thus, 1-D external losses were estimated and combined with stage efficiency obtained from CFD.

The pressure ratios are higher in the CFD result. The authors think that some of the internal losses in the CFD were reduced than the real system although the mesh system is converged.

In addition, the contour plot of static pressure at the 35,000rpm was made to see whether subcritical region exist or not. The minimum pressure at the leading edge is 7.52MPa, which maintains supercritical state.

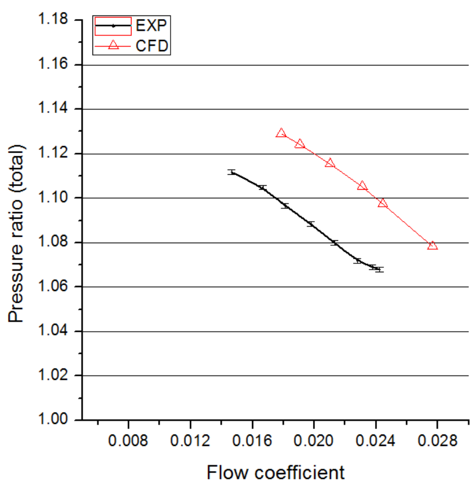

Fig. 6. Comparison of pressure ratio versus flow coefficient.

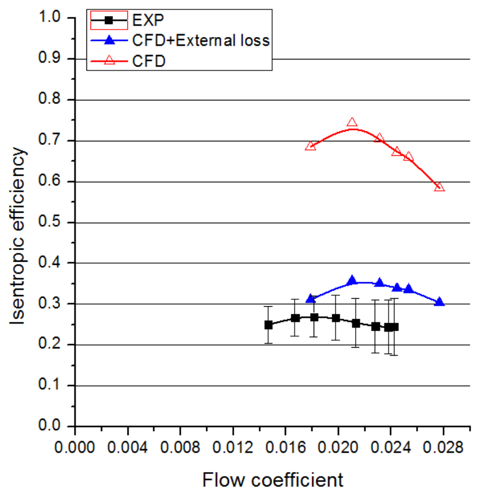

Fig. 7. Comparison of isentropic efficiency versus flow coefficient.

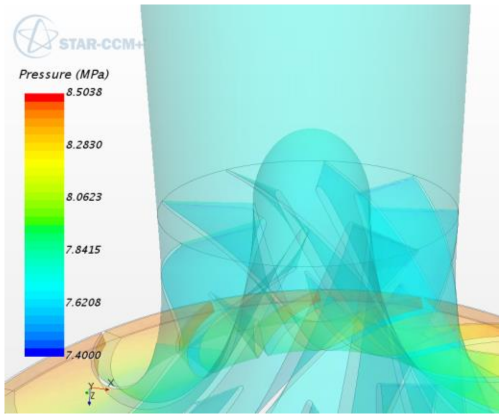

Fig. 8. Static Pressure distribution at the leading edge.

6. Conclusions

RANS simulation of a S-CO_2 compressor was presented in this study. Accurate properties of S-CO_2 are implemented to the Star-CCM+ code as a CSV table format file. The compressor testing data obtained from SCIEL facility were compared to the CFD results. In addition, external losses including disk friction, rotor cavity, and leakage flow were considered to compare performance result with experiment.

ACKNOWLEDGEMENT

Authors gratefully acknowledge that this research is financially supported by the National Research Foundation of Korea (NRF) and funded by the Korean Ministry of Trade, Industry and Energy (MOTIE).

REFERENCES

[1] Vaclav Dostal, Michael J. Driscoll, and Pavel Hejzlar. "A supercritical carbon dioxide cycle for next generation nuclear reactors." Massachusetts Institute of Technology. Dept. of Nuclear Engineering, Cambridge, MA, Paper No. MIT-ANP-TR-100 (2004).

[2] Y. Ahn, J. Lee, S. G. Kim, J. I. Lee, J. E. Cha, The Design Study of Supercritical Carbon Dioxide Integral Experiment Loop, Proceedings of ASME Turbo Expo 2013, San Antonio, Texas, USA, 2013.

[3] J. E. Cha, S. W. Bae, J. Lee, S. K. Cho, J. I. Lee, J. H. Park, “Operation results of a closed supercritical CO2 simple Brayton cycle”, The 5th international symposium – supercritical CO2 Power cycles, March 25-31, 2016, San Antonio, Texas.

[4] Smirnov, Pavel E., and Florian R. Menter. "Sensitization of the SST turbulence model to rotation and curvature by applying the Spalart–Shur correction term." Journal of Turbomachinery 131.4 (2009): 041010.

[5] Luca Mangani, Ernesto Casartelli, Sevastiano Mauri, Assessment of Various Turbulence Models in a High Pressure Ratio Centrifugal Compressor with an Object Oriented CFD Code, Journal of Turbomachinery 134 (2012).

[6] Z. Liu, D. L. Hill, “Issues Surrounding Multiple Frames of Reference Models for Turbo Compressor Applications” (2000). International Compressor Engineering Conference. Paper 1369.

[7] Celik, Ishmail B., Urmila Ghia, and Patrick J. Roache. "Procedure for estimation and reporting of uncertainty due to discretization in {CFD} applications." Journal of fluids {Engineering-Transactions} of the {ASME} 130.7 (2008).

[8] Jekyoung Lee, Study of improved design methodology of S-CO2 power cycle compressor for the next generation nuclear system application, Ph.D Thesis, Korea Advanced Institute of Science and Technology, June 2016.

[9] Daily, James W., and Ronald E. Nece. "Chamber dimension effects on induced flow and frictional resistance of enclosed rotating disks." Journal of basic engineering 82.1 (1960): 217-230.

[10] J. F. Gulich, “Disk friction losses of closed turbomachine impellers”, Forsching im Ingenieurwesen 68 (2003) 87-95.

[11] J. E. Vrancik, “Prediction of windage power loss in alternators”, Lewis Research Center, NASA Technical Note, NASA TN D-4849 (1968).

[12] H. Schlichting, Boundary-Later Theory, Seventh Edition, McGRAW-HILL (1979).